Glucocorticoid Receptor (GR) Activation Is Associated with Increased cAMP/PKA Signaling in Castration-Resistant Prostate Cancer

Lynda Bennett[1], Praveen Kumar Jaiswal[1], Ryan V. Harkless[1], Tiha M. Long[2], Ning Gao[1], Brianna Vandenburg[1], Phillip Selman[2], Ishrat Durdana[1], Ricardo R. Lastra[3], Donald Vander Griend[4], Remi Adelaiye-Ogala[5], Russell Z. Szmulewitz[2], and Suzanne D. Conzen[1]

ABSTRACT

In castration-resistant prostate cancer (CRPC), increased glucocorticoid receptor (GR) expression and ensuing transcriptional activity have been proposed as an oncogenic "bypass" mechanism in response to androgen receptor (AR) signaling inhibition (ARSi). Here, we report that GR transcriptional activity acquired following ARSi is associated with the upregulation of cyclic adenosine monophosphate (cAMP)-associated gene expression pathways in both model systems and metastatic prostate cancer patient samples. In the context of ARSi, the expression of GR-mediated genes encoding cAMP signaling pathway-associated proteins can be inhibited by treatment with selective GR modulators (SGRMs). For example, in the context of ARSi, we found that GR activation resulted in upregulation of *protein kinase inhibitor beta* (*PKIB)* mRNA and protein levels, leading to nuclear accumulation of the cAMP-dependent protein kinase A catalytic subunit (PKA-c). Increased PKA-c, in turn, is associated with increased cAMP response element-binding protein phosphorylation and activity. Furthermore, enzalutamide and SGRM combination therapy in mice bearing CRPC xenografts delayed CRPC progression compared with enzalutamide therapy alone, and reduced tumor *PKIB* mRNA expression. Supporting the clinical importance of GR/PKA signaling activation in CRPC, we found a significant enrichment of both cAMP pathway signaling-associated gene expression and high *NR3C1* (GR) activity in patient-derived xenograft models and metastatic human CRPC samples. These findings suggest a novel mechanism linking CRPC-induced GR transcriptional activity with increased cAMP signaling in AR-antagonized CRPC. Furthermore, our findings suggest that GR-specific modulation in addition to AR antagonism may delay GR+ CRPC time to recurrence, at least in part, by inhibiting tumor cAMP/PKA pathways.

Introduction

Prostate cancer is the most commonly diagnosed and the second leading cause of cancer death in men in the United States (1). Prostate cancer progression is primarily driven by androgen receptor (AR) activity (2), and medical castration with AR antagonism is the mainstay treatment for metastatic prostate cancer. Nevertheless, almost all prostate cancer progresses into "castration-resistant" prostate cancer (CRPC; ref. 3). While the addition of second-generation AR antagonists, including enzalutamide, prolongs patient survival, prostate cancer progression inevitably occurs despite castration and AR pathway/signaling inhibition (ARSi; refs. 4, 5).

A proposed mechanism of prostate cancer resistance to ARSi involves increased glucocorticoid receptor (GR) expression and/or GR-mediated transcriptional activity following ARSi (6, 7). In several types of cancer, our group and others previously discovered that activated tumor GR signaling promotes cancer cell survival and other pro-oncogenic functions (8, 9). In prostate cancer, increased GR transcriptional activity has been proposed to overcome ARSi by acting as an "AR-bypass" mechanism. Because of the significant homology between AR and GR, activated GR can bind several shared DNA response elements (e.g., both AREs and GREs) and regulate the transcription of a subset of the same target genes. For example, we previously showed that GR activation in AR-antagonized prostate cancer cells induces the expression of several pro-proliferative AR target genes, and that selective GR modulation/antagonism reverses this common AR/GR-mediated gene regulation. Although this "bypass of AR blockade by activated GR" mechanism is likely an important component of GR activity in CRPC, the contribution of additional GR target gene expression pathways that are distinct from canonical AR transcriptional activity has not been well studied.

Here, we identify examples of GR-mediated gene expression pathways that are: (i) acquired after AR antagonism, (ii) are distinct from AR-mediated gene expression pathways, and (iii) may contribute to CRPC progression independently of simply recapitulating AR activity. Using two prostate cancer cell lines cultured *in vitro*, analysis of the GR-activated transcriptome following several days of enzalutamide (ARSi) treatment revealed that cyclic adenosine monophosphate (cAMP)-mediated signaling and protein kinase A (PKA) signaling were among the most significantly activated GR-mediated gene expression pathways emerging in the AR-antagonized context.

[1]Division of Hematology and Oncology, Department of Internal Medicine, UT Southwestern Medical Center, Dallas, Texas. [2]Section of Hematology and Oncology, Department of Medicine, The University of Chicago, Chicago, Illinois. [3]Department of Pathology, The University of Chicago, Chicago, Illinois. [4]Department of Pathology, University of Illinois at Chicago, Chicago, Illinois. [5]Division of Hematology and Oncology, Jacobs School of Medicine and Biomedical Sciences, University of Buffalo, Buffalo, New York.

L. Bennett, P.K. Jaiswal, R.V. Harkless, and T.M. Long contributed equally to this article.

Corresponding Authors: Suzanne D. Conzen, Division of Hematology and Oncology, UT Southwestern Medical Center, Dallas, TX 75390. E-mail: suzanne.conzen@utsouthwestern.edu; and Russell Z. Szmulewitz, Section of Hematology/Oncology, The University of Chicago, Chicago, IL 60637. E-mail: rszmulew@medicine.bsd.uchicago.edu

Mol Cancer Ther 2024;23:552–63

doi: 10.1158/1535-7163.MCT-22-0479

Consistent with this observation, both increased cAMP/PKA signaling (10) and increased GR activity (11), have been previously observed as associated with androgen deprivation therapy resistance in CRPC. We found that GR-mediated gene expression regulated after CRPC included *protein kinase inhibitor beta* (*PKIB)* and other genes encoding proteins essential for PKA pathway activation. *In vivo* and *in vitro*, addition of a highly selective GR modulator (SGRM) resulted in decreased *PKIB* tumor cell gene expression, suggesting that acquired GR oncogenic pathways may be blocked by GR-specific antagonism. Using *in vivo* tumor gene expression data from a CRPC patient-derived xenograft (PDX) mouse model and patient prostate cancer metastases, we found that increased GR activation is accompanied by significantly increased cAMP/PKA pathway gene activation. Thus, we propose a model in which ARSi results in newly acquired GR CRPC transcriptional activity that includes the induction of PKA oncogenic activity.

Materials and Methods

Cell culture

LAPC4 and CWR-22Rv1 were a generous gift of Dr. John Isaacs (Johns Hopkins University) and routinely authenticated using short tandem repeat profiling (DDX Medical). Cells were similarly tested twice a year for *Mycoplasma* contamination using the American Type Tissue Culture Universal Mycoplasma Detection Kit. LAPC4 cells were grown in IMDM (Hyclone) supplemented with 1% penicillin/streptomycin (Gibco), 10% FBS (Gemini Bio-Products), and 1 nmol/L R1881 (Sigma-Aldrich). CWR-22Rv1 cells were grown in RPMI1640 (Gibco) supplemented with 1% penicillin/streptomycin (Gibco) and 10% FBS (Gemini Bio-Products).

Cell treatments

Cells were plated in standard media, as described above, and incubated overnight. Cells were washed with PBS (Hyclone) and placed in medium containing 10% charcoal-stripped FBS (Atlanta Biologicals). Cells were treated for the indicated times with media changes every 2 to 3 days with either vehicle control or specified treatment: 1 nmol/L R1881 (Sigma-Aldrich), 100 nmol/L dexamethasone (MP Biomedicals), 10 μmol/L enzalutamide (Selleck Chemicals or Medivation), 100 nmol/L mifepristone (Sigma-Aldrich), 1 μmol/L of compounds CORT118335, CORT108297 (Corcept Therapeutics), or 10 μmol/L forskolin (Cayman Chemical). For all experiments, an equimolar amount of vehicle (ethanol or DMSO) was added to each sample for equal treatment periods.

Protein lysate preparation and immunoblotting

Cells were lysed in radioimmunoprecipitation assay (RIPA) buffer and sonicated. Xenograft tumor cell lysates were prepared similarly, with an additional step of homogenization. Protein concentration was determined using the Pierce BCA Protein Assay Kit (Thermo Scientific), and lysates containing 50 to 100 μg of protein were loaded onto gels, resolved, and transferred to nitrocellulose membranes (LI-COR). Membranes were blocked in 5% BSA, incubated with the indicated primary antibody overnight, and washed. Fluorescently-labeled secondary antibodies (1:10,000, LI-COR) were incubated and washed. Detection was performed using the LI-COR Odyssey or Bio-Rad Chemidoc MP Imaging systems. Antibodies and concentrations were: anti-pan-phospho-PKA substrate [100G7E, 1:1,000, Cell Signaling Technology (CST)], anti-phospho-cAMP response element-binding protein (CREB) Ser133 (87G3, 1:1,000, CST), anti-CREB (86B10, 1:1,000, CST), anti-α-tubulin (DM1A, 1:5,000, CST), anti-beta actin (8H10D10, 1:5,000, CST), anti-PKA catalytic subunit (anti–PKA-c; 1:1,000, Santa Cruz Biotechnology sc-28315), anti-PKIB (1:1,000, Abcam ab233521), anti-Vinculin (13901, 1:1,000, CST), anti-Lamin B1 (13435, 1:1,000, CST). Positive control lysates for PKIB immunoblotting were from LAPC4 and CWR-22Rv1 cells transiently transfected with a human *PKIB* plasmid (NM_001270395, catalog no. RC231584). Nuclear and cytoplasmic fractionation was performed using a commercial nuclear extraction kit (Active Motif, 40410) using LAPC4 and CWR-22Rv1 cells cultured for 3 days with 1 nm R1881 and 10 μmol/L enzalutamide (ARSi) and then treated either with vehicle or dexamethasone (100 nm) for the last 8 hours. Lysates were processed for Western blotting as above and bands were quantified using LICOR-Image studio and Image J software.

RNA extraction and quantitative reverse transcription—PCR

RNA was extracted from lysed cells using the RNeasy Mini Kit (Qiagen). Tumor RNA was extracted using the RNeasy Midi Kit (Qiagen). Minced tumors (∼100 mg pieces) were homogenized using a TissueLyser LT (Qiagen) and a TissueLyser single bead dispenser 5 mm (Qiagen). DNA digestion was performed using a Qiagen RNase-free DNase set. RNA concentrations were measured with a NanoDrop One (Thermo Scientific), or a Qubit 4 Fluorometer (Invitrogen Thermo Fischer Scientific). cDNA was synthesized using Superscript IV VILO Master Mix (Invitrogen), and real-time PCR was performed using QuantStudio 6 Pro (Applied Biosystems) with TaqMan Fast Advanced Master Mix (Applied Biosystems). Probes used were *PKIB* (Hs00261162_m1) and *ACTB* (Hs99999903_m1) as control. The standard deviation between replicates was less than 0.15. To evaluate the integrity of tumor RNA, we determined the RNA Integrity Number (RIN) score and *ACTB* expression in each tumor sample. Tumor samples were considered to be degraded and were excluded from analysis if the RIN score was below 4.5 or if the *ACTB* expression deviated ± 1.5-fold from the average *ACTB* expression within each treatment group. Experiments were repeated at least 3 times with consistent results, and one biological replicate was chosen for representation.

Immunofluorescence

Cells were fixed on glass slides using 3.7% formaldehyde for 10 minutes and incubated for 1 hour in blocking buffer (5% normal goat serum and 0.01% Triton-x100), primary antibody (1:100), and secondary antibody (1:500). The cells were mounted in medium containing the DAPI and observed under 600X magnification with a Nikon Ti2 Eclipse microscope. The light source intensity, aperture, and exposure time were kept consistent between samples. The following antibodies and reagents were used: anti-PKA-c (Santa Cruz Biotechnology, sc-28315), anti-PKIB (ThermoFisher Scientific, PA538783), anti-CREB (CST, 9104), anti-phospho-CREB S133 (CST, 9198), goat anti-rabbit and anti-mouse secondary antibodies (ThermoFisher Scientific, A32732, A32723), mounting medium with DAPI (ThermoFisher Scientific, P36941), and normal goat serum (CST, 5425S).

Quantification of mean immunofluorescence intensity

NIS-Elements Imaging Software was used for immunofluorescence intensity quantification. Images were first deconvoluted, and then subcellular masks were created. Nuclear and whole cell masks were generated in each field of view (FOV) by outlining all nuclei or whole cell areas, respectively. The cytoplasmic mask was created using the nonequivalence function, which subtracts the nuclear from the whole-cell component. The mean immunofluorescence intensity for each cellular component (nuclear, cytoplasmic, and whole cell) was

calculated for each FOV. Eight to thirteen FOVs were measured for each condition.

RNA sequencing and analysis

Total RNA was isolated using the RNeasy Mini Kit (Qiagen), following the manufacturer's instructions. The quality of the extracted RNA was evaluated using the 2200 TapeStation system (Agilent). Samples with a RIN score of ≥7 were selected for library preparation. RNA sequencing (RNA-seq) libraries were built using the 'Stranded mRNA-Seq' Kit for Illumina platforms (KAPA) with OligodT magnetic beads to enrich for mRNA species. Libraries were run on a 2200 TapeStation (Agilent) to confirm fragment size and then quantified by qPCR using the Library Quantification kit (KAPA). Sequencing was performed on a HiSeq 2000 (Illumina) in 100bp, paired-end runs. The quality of raw reads was assessed using FastQC (http://www.bioinformatics.babraham.ac.uk/projects/fastqc; v0.11.4). Sequencing reads were mapped to the human genome assembly (UCSC hg19) using STAR (ref. 12; v2.5.2b). Alignment metrics were collected using Picard tools (v2.8.1) (http://broadinstitute.github.io/picard/) and RSeQC (ref. 13; v2.6.4). The resulting files from the previous alignment step in the RNA-seq analysis were taken individually as input to quantify transcriptional expression using fragments per kilobase of transcript per million mapped reads (FPKM)-based and read count-based methods. Differentially expressed genes (DEG) and isoforms were detected using the Cuffquant-Cuffnorm-Cuffdiff (ref. 14; v2.2.1) suite (FPKM-based method) and Rsubread::featureCounts (ref. 15; v1.24.2)-DESeq2 (ref. 16; v1.14.1) or edgeR (ref. 17; v3.16.5; read count-based method). DEGs identified using fold change ≥ 1.3 were analyzed with ingenuity pathway analysis (IPA; Qiagen Inc., https://digitalinsights.qiagen.com/products-overview/discovery-insights-portfolio/analysis-and-visualization/qiagen-ipa/?cmpid=QDI_GA_DISC_IPA&gad_source=1&gclid=CjwKCAjwkuqvBhAQEiwA65XxQMiHSmK6tW1iTNhn-SaSqHcapyY_vptMCG0pn_cUqpS0aSwzpPtcBBoCSjcQAvD_BwE) to identify functional categories or pathways that were significantly altered under various conditions. Heat maps were generated from IPA activation Z-scores and/or *P* values using Morpheus software (https://software.broadinstitute.org/morpheus/).

Normalization of metastatic prostate cancer RNA-seq data

We obtained raw RNA-Seq FASTQ files of 25 primary prostate tumors and 99 CRPC metastases using dbGAP (phs000310.v1.p1 for tumors and benign glands; phs000915.v1.p1 for metastases; refs. 18, 19). The same RNA-seq analysis described in the previous section was applied to these downloaded reads. Here, transcripts were selected using fold change ≥1.5 for further analyses. To select DEGs based on GR expression in metastatic CRPC (mCRPC), metastatic tumors were selected by the upper and lower quartiles of GR expression. A Mann–Whitney–Wilcox comparison was performed for each gene between these two groups, and significant genes were selected with a P value of <0.05 after correction for multiple testing using the Benjamini-Hochberg method. Biological insights from candidate gene lists were obtained by performing gene set enrichment analysis (GSEA) using the Broad Institute GSEA 3.0 software and IPA (Qiagen) to identify functional categories or pathways that were significantly altered in the DEGs.

GSEA was performed using the Broad Institute GSEA 4.2.2 software (20) and an expanded dataset of RNA-seq from 118 metastatic prostate cancers. RPKM from polyA mRNA expression data was downloaded from cBioPortal.org (http://www.cbioportal.org/study/summary?id=prad_su2c_2015). Normalized values (TPM) were extracted using default settings in EdgeR, and the upper and lower quartiles for *NR3C1* expression (GR-high and GR-low; 29 samples per group) were used for GSEA. A custom cAMP pathway gene set was created using IPA software (Qiagen) and GSEA was performed along with the Human MSigDB Hallmark gene set (BROAD Institute).

Animal studies

Animal studies were carried out in compliance with the U.S. Public Health Service Policy on Humane Care and Use of Laboratory Animals and were approved by The University of Chicago Institutional and Animal Care and Use Committee. Male nude mice (8–10 weeks old, Envigo) were castrated and implanted with approximately 25 mg testosterone (4-androsten-17β-OL-3-ONE, Steraloids) loaded into a 1 cm "pellet" of silastic tubing to maintain consistent and equivalent levels of testosterone in all mice similar to the physiologic concentration of testosterone in humans. Testosterone implants elevate and maintain testosterone levels to 530 ± 50 ng/dL (18.2 nmol/L), which is similar to that in eugonadal adult human males (21). One week later, mice were injected subcutaneously in the flank with 1×10^6 LAPC4 prostate cancer cells in 100 μL 75% Matrigel (Corning) and 25% HBSS (Gibco). Testosterone pellets were removed (castration) when the tumors reached a size of ∼250 mm^3. Mice were treated following "castration resistance," as indicated by tumor doubling (∼500 mm^3). Mice received daily intraperitoneal injections of vehicle or 20 mg/kg of the Corcept compound dissolved in ethanol and diluted 1:10 v/v in sesame oil (Sigma) in combination with enzalutamide 30 mg/kg chow (OpenSource Diets). Treatment was continued until CRPC progression, defined as tumor doubling relative to size at treatment initiation. Time-to-endpoint Kaplan–Meier curves were generated using GraphPad Prism and compared using the Grehan–Breslow–Wilcoxon test to determine statistical significance. A subset of mice was also sacrificed at the time of castration, treatment initiation, 1 week of treatment, and at the endpoint of tumor doubling. Tumors were harvested and frozen for protein analysis, stored in RNAlater (Qiagen) for RNA extraction, and formalin-fixed for paraffin embedding.

Immunohistochemistry

Formalin-fixed, paraffin-embedded tumors were cut into 5 μm section slides and stained with hematoxylin and eosin, anti-GR (D8H2, 1:1,500, CST), and anti-Ki67 (D3B5, #12202 1:400, CST). The slides were scored by a pathologist (RL) blinded to the treatment conditions. Anti-Ki67 IHC slides were scanned on a Leica Aperio (Leica Biosystems). Images were viewed on Leica Aperio ImageScope software and 200X digital images were used for publication. Percentages of Ki67+ cells were determined using QuPath (22).

Data availability

The sequencing data generated in this study are publicly available in NCBI Gene Expression Omnibus at Accession # GSE97204

Prostate cancer patient data analyzed in this study were obtained from cBioPortal.org at http://www.cbioportal.org/study/summary?id=prad_su2c_2015

Results

In AR-antagonized (ARSi) prostate cancer, a significant subset of GR-regulated genes is distinct from the AR-activated transcriptome

Increased GR expression/activity in AR-antagonized prostate cancer models and human samples has been described previously as an "AR-bypass" mechanism (6, 7, 9). However, GR-driven/AR-distinct molecular pathways involved in GR-associated CRPC progression may contribute to prostate cancer evolution. In particular, it is unclear

whether GR solely recapitulates AR-driven oncogenic mechanisms or whether GR activation also regulates newly expressed, GR-unique (i.e., different from AR) pathways, allowing an additional metastatic advantage for GR+ CRPC. To investigate GR activity in a cell culture system that is physiologically relevant to clinical CRPC, we first cultured cells in media containing androgen and enzalutamide to mimic AR antagonism in patients' tumors, and then measured GR-specific gene expression following GR agonist (Dex) treatment (**Fig. 1A**). To determine the overlap between genes regulated by GR activation in the ARSi context versus genes regulated by AR activation in the same cells, LAPC4 cells were treated with androgen (R1881, R) and enzalutamide (E) for 3 days followed by the addition of dexamethasone (dex) for 6 hours and resulting gene expression compared with the transcriptome of AR-activated genes (i.e., R vs. V). RNA from each sample was isolated for next-generation sequencing and mapped to the human genome, and mRNAs that were up- or downregulated >1.3-fold were defined as DEGs. Androgen (R1881) treatment up- or downregulated the expression of 5,920 genes > 1.3-fold compared with vehicle-treated LAPC4 cells (i.e., AR transcriptome). The addition of dex to AR-antagonized cells resulted in the regulation of 4,692 genes in LAPC4 cells. We identified AR/GR shared DEGs by overlapping genes that were upregulated or downregulated by androgen and similarly regulated (same directionality) by dex in the AR-antagonized (ARSi) state. Of note, 40% of GR-regulated genes ($N = 1,860$) were GR-unique (i.e., did not overlap with AR DEGs), suggesting an additional role for a significant subset of the GR transcriptome beyond simply recapitulating AR signaling (**Fig. 1A**, left). To determine whether a significant subset of GR- and AR-induced gene expression was similarly non-overlapping in a second prostate cancer cell line, CWR-22Rv1 cells, which are derived from the lymph node of a castrated mouse and have much higher baseline GR, were examined under identical conditions. In CWR-22Rv1 cells, AR activation alone resulted in the differential expression of 5697 genes. Addition of dex to AR-antagonized cells (i.e., **R**1881, **E**nza for 3 days followed by **D**ex activation for 6 hours, or **RED**) modulated the expression of 3,976 genes. Similar to the results in LAPC4 cells, 41% of RED versus RE DEGs (i.e., ARSi GR-transcriptome) were GR-unique ($N = 1,632$; **Fig. 1A**, right). That is, these GR-mediated genes did not overlap with the AR target genes. The heat map in **Fig. 1B** shows all RED GR DEGs compared with the AR transcriptome and reveals the relatively modest overlap of GR and AR DEGs in both LAPC4 and CWR-22Rv1 cell lines. Taken together, these data suggest that GR transcriptional activity (subsequent to ARSi) extends well beyond simply recapitulating AR-mediated gene expression.

SGRMs antagonize the expression of the majority of GR-regulated genes in AR-antagonized (ARSi) prostate cancer cells

We previously demonstrated that in prostate cancer models subjected to AR antagonism, adding SGRMs CORT108297 (ref. 23; C297) and CORT118335 [(24) compound 7] (C335, miricorilant) inhibits most (but not all) GR transcriptional activity (9). In this study, to determine whether SGRMs inhibit GR transcriptional regulation of genes that do not overlap with the AR-mediated transcriptome, LAPC4 and CWR-22Rv1 cells were treated as above with androgen (R) and enzalutamide (E) (3 days followed by a 6-hour pulse of Dex ± co-treatment with 6 hours of either SGRM C297 or C335). RNA-seq data from RED- vs. RED+SGRM-treated cells were analyzed in both LAPC4 and CWR-22RV1 cells (**Fig. 1C**). In LAPC4 cells, addition of either SGRM C297 or C335 reversed the dex-induced up- or downregulation of ∼80% of GR/AR shared genes. Both SGRMs also reversed up- or downregulation of 81% of GR-unique genes (**Fig. 1C**, top). In CWR-22Rv1 cells, the addition of a SGRM reversed the dex-induced upregulation or downregulation of 62% (C297) and 89% (C335) of GR/AR shared genes. Similarly, SGRMs reversed the up- or downregulation of 82% (C297) and 86% (C335) of GR-unique genes (**Fig. 1C**, bottom). In summary, GR activity following ARSi regulates a significant subset of genes that do not overlap with the AR transcriptome, and importantly, SGRMs are effective at antagonizing GR-regulation independently of whether these genes are also AR-regulated or GR-unique.

cAMP/PKA signaling pathways are induced by GR activation in ARSi prostate cancer

To further understand the downstream biology resulting from GR-mediated gene expression pathways in prostate cancer, we applied the IPA program to GR-mediated gene expression following ARSi (25). We found that GR activation pathways were implicated in cAMP/PKA-mediated signaling in both cell lines and relatively repressed with Dex+C297 or DEX+C335 treatments (Supplementary Tables S1 and S2). A closer investigation of the GR-activated gene expression pathways in LAPC4 cells revealed that the majority of the 224 genes (Supplementary Table S3) in the canonical IPA "cAMP-mediated signaling pathway" were either significantly up- or down-regulated (>1.3-fold) by the addition of dex. Furthermore, the addition of either SGRM C297 or C335 antagonized the majority of the GR-mediated cAMP-pathway genes (**Fig. 2A**). Similarly, in CWR-22Rv1 cells, the majority of the cAMP-mediated signaling pathway genes were found to be regulated by GR activation (Supplementary Fig. S1A).

It has been previously reported that the cAMP/PKA signaling pathway contributes to prostate cancer ARSi resistance (26). Because GR-mediated gene regulation following ARSi suggested activation of the cAMP/PKA pathways (Supplementary Tables S1 and S2), we first investigated whether GR activation generally increased PKA-mediated phosphorylation events by performing a pan-phospho-PKA substrate Western blot in CWR-22Rv1 cells treated ± dex (Supplementary Fig. S2). This Western blot suggested an increase in PKA substrate phosphorylation following GR activation with dex (a band the size of pCREB, a canonical substrate of PKA is shown with an asterisk in Fig. S2). It had also been shown previously that PKIB protein expression in prostate cancer cells is associated with an increase in PKA-mediated substrate phosphorylation and prostate cancer progression (27). Therefore, we asked whether *PKIB* expression might be upregulated following GR activation (**Fig. 2B**; Supplementary Fig. S1B). Indeed, we found that *PKIB* steady-state mRNA expression was relatively increased in both LAPC4 and CWR-22Rv1 cells following GR activation. The co-treatment of either SGRM decreased the expression of *PKIB* relative to dex treatment alone. Furthermore, in both LAPC4 and CWR-22Rv1 cells, PKIB protein expression increased following GR activation and was relatively decreased by concomitant treatment with a SGRM (Western blot; **Fig. 2B**; Supplementary Figs. S1B, S3A and S3B).

Increased GR-mediated PKIB expression is associated with nuclear sequestration of catalytically active PKA (PKA-c) and a subsequent increase in PKA activity

PKIB sequesters the PKA-c in the nucleus, resulting in increased PKA activity (27). Therefore, we evaluated PKIB nuclear expression in AR-antagonized prostate cancer cells before and after GR activation. Examination of dex-treated (GR-activated) cells revealed a relative increase in nuclear PKIB expression following GR activation (LAPC4 cells $P < 0.0001$; **Fig. 2C** and CWR-22Rv1 cells $P < 0.05$; Supplementary Fig. S1C). We next investigated whether the GR activation-

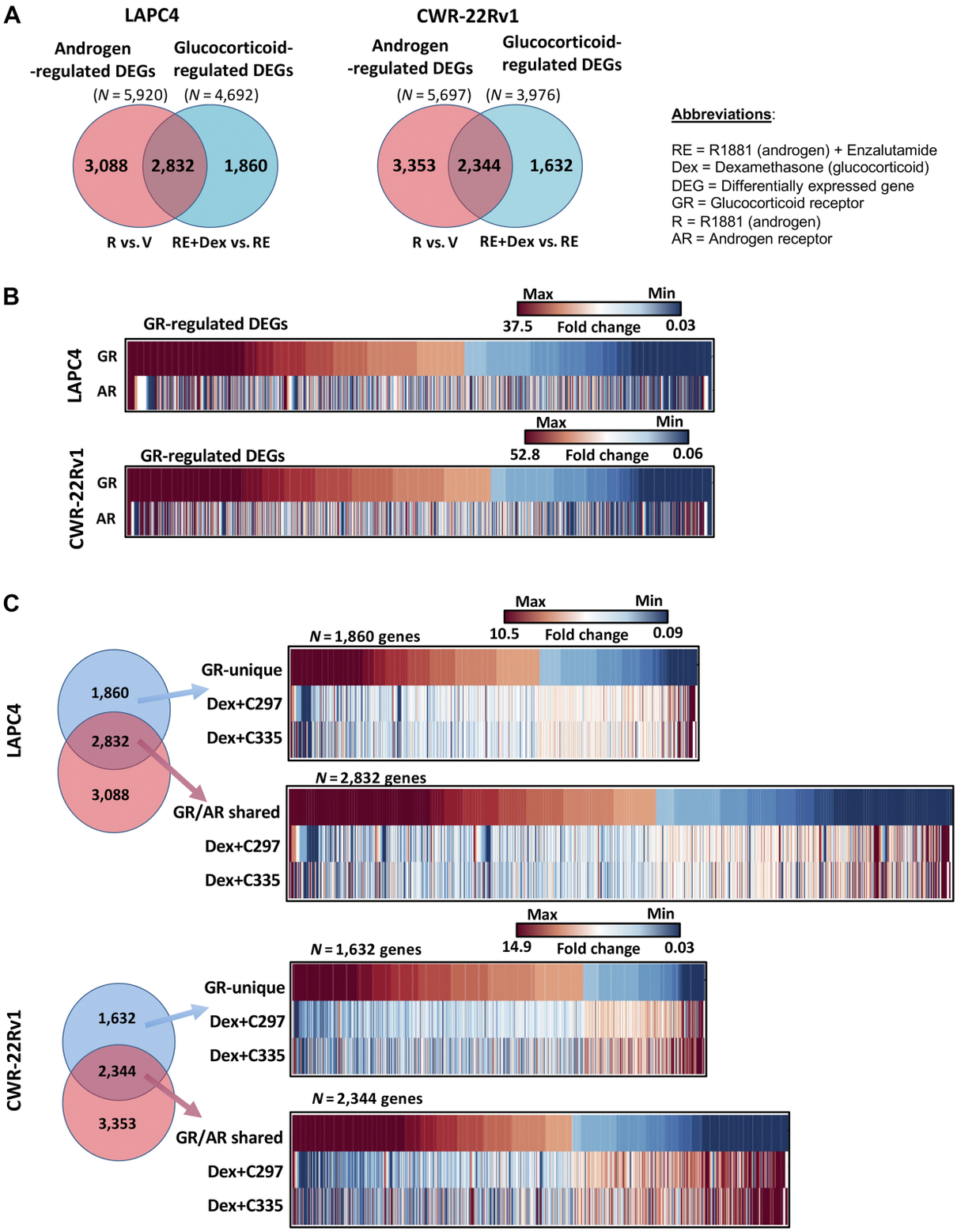

Figure 1.

Following AR antagonism, SGRMs antagonize expression of both GR/AR shared (overlapped) as well as GR uniquely regulated genes. **A,** Venn diagrams of LAPC4 (left) and CWR-22Rv1 (right) cell lines show AR-mediated DEGs (up- or downregulated ≥ 1.3-fold following androgen (R1881, red color) or dexamethasone (GR)-regulated genes (RED = RE+Dex vs. RE, blue color). **B,** Heat maps of GR-regulated genes and AR-regulated genes for LAPC4 and CWR-22Rv1 cell-lines. **C,** Heat maps for LAPC4 (top) and CWR-22Rv1 cells (bottom) GR-unique genes (no overlap with AR cistrome) and their expression following co-treatment with Dex + SGRMs (C297 or C335). Scale shows maximum/minimum fold-change gene expression for GR-regulated DEGs.

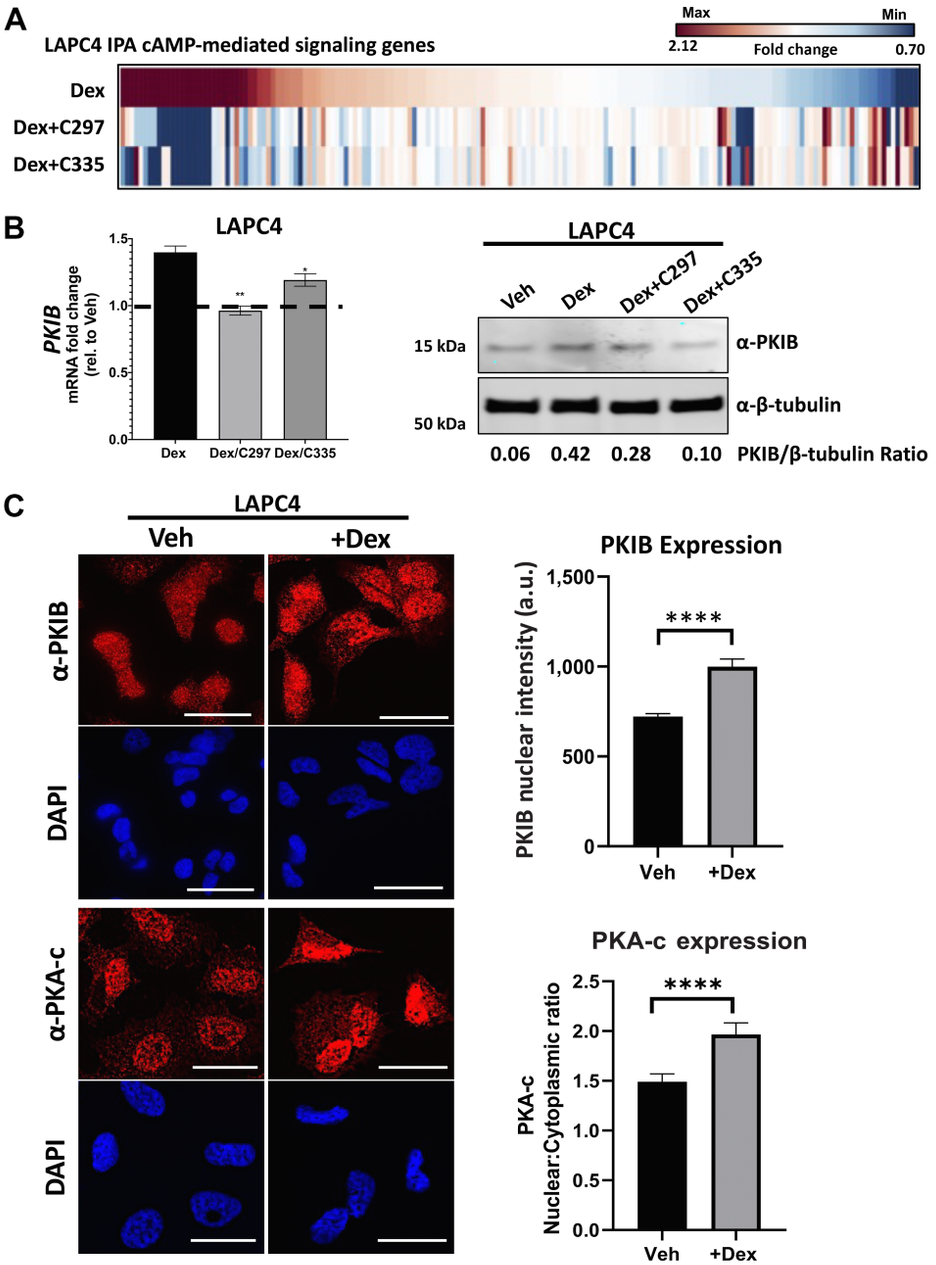

Figure 2.

GR-mediated cAMP signaling pathway-related genes (n = 224) with co-treatment of SGRMs. **A,** Heat map of IPA "cAMP signaling pathway gene expression" in LAPC4 cells treated with Dex and ± GR antagonism (as in **Fig. 1C**). **B,** LAPC4 cells were cultured in media containing R1881 and enzalutamide for 7 days, and then treated for 6 hours with either Veh, Dex, Dex+C297, or Dex+C335 and qRT-PCR was performed for a cAMP pathway gene previously associated with prostate cancer biology (27), *PKIB*. *PKIB* steady-state mRNA expression (left: *, $P < 0.05$; **, $P < 0.005$; Welch t test). Western blot was performed for PKIB protein expression (right). Densitometric analysis of PKIB vs. β-tubulin is shown below each lane (Western blot is representative of three independent experiments which are quantified in Supplementary Fig. S3A). **C,** Left, LAPC4 cells were cultured as above, and then treated with ± Dex (8 hours). Cells were probed with either α-PKIB (top) or α-PKA-c antibody (third row) and counterstained with DAPI (600X magnification, scale bar = 25 μm). Right, Bar graph of nuclear PKIB expression per FOV (top) and the ratio of the average PKA-c nuclear to cytoplasmic intensity per FOV following Veh or Dex treatment (bottom). FOV (8–13) per condition were measured for average intensity: a.u., arbitrary unit; ****, $P < 0.0001$ (Welch t test).

induced PKIB was associated with increased PKA-c accumulation. LAPC4 and CWR-22Rv1 cells were treated as above and probed for PKA-c using indirect immunofluorescence. GR activation resulted in increased nuclear sequestration of PKA-c in LAPC4 ($P < 0.0001$; **Fig. 2C**) and CWR-22Rv1 cells ($P < 0.0001$; Supplementary Fig. S1C). We also examined subcellular localization of activated PKA substrates, including CREB, PKA-c, and PKIB by nuclear-cytoplasmic fractionation and Western blotting. Upon GR activation (dex treatment), we observed an increase in pCREBs133, CREB, PKA-c, and PKIB proteins within the nuclear fraction in LAPC4 and CWR-22Rv1 cells (**Fig. 3A**; Supplementary Fig. S4A). Taken together, these data suggest that GR activation (following AR antagonism) increases PKIB protein expression in association with nuclear sequestration of PKA-c, which is, as expected, accompanied by an increase in pCREB expression.

To probe more specifically, LAPC4 and CWR-22Rv1 cells were cultured for 7 days with 1 nmol/L R1881 (R), 1 nmol/L R1881 with 10 μmol/L enzalutamide (RE) and then treated for 8 hours with vehicle, 100 nmol/L dex, or dex with either 1 μmol/L SGRM C297 or C335. As CREB-serine133 (CREBs133) phosphorylation following androgen deprivation is associated with its activation (28), whole-cell lysates were analyzed by immunoblotting with anti-phospho-CREBs133, anti-GR, and anti-AR. Indeed, we found that CREBs133 phosphorylation increased following GR activation (**Fig. 3B**; Supplementary Fig. S4B). This was confirmed by immunofluorescence microscopy of pCREBs133 (**Fig. 3C**; Supplementary Fig. S4C). Furthermore, we examined GR and AR protein levels and found no significant effects from either Dex or Dex +C297/C335 (**Fig. 3B**; Supplementary Fig. S4B). In addition, immunoblotting revealed that

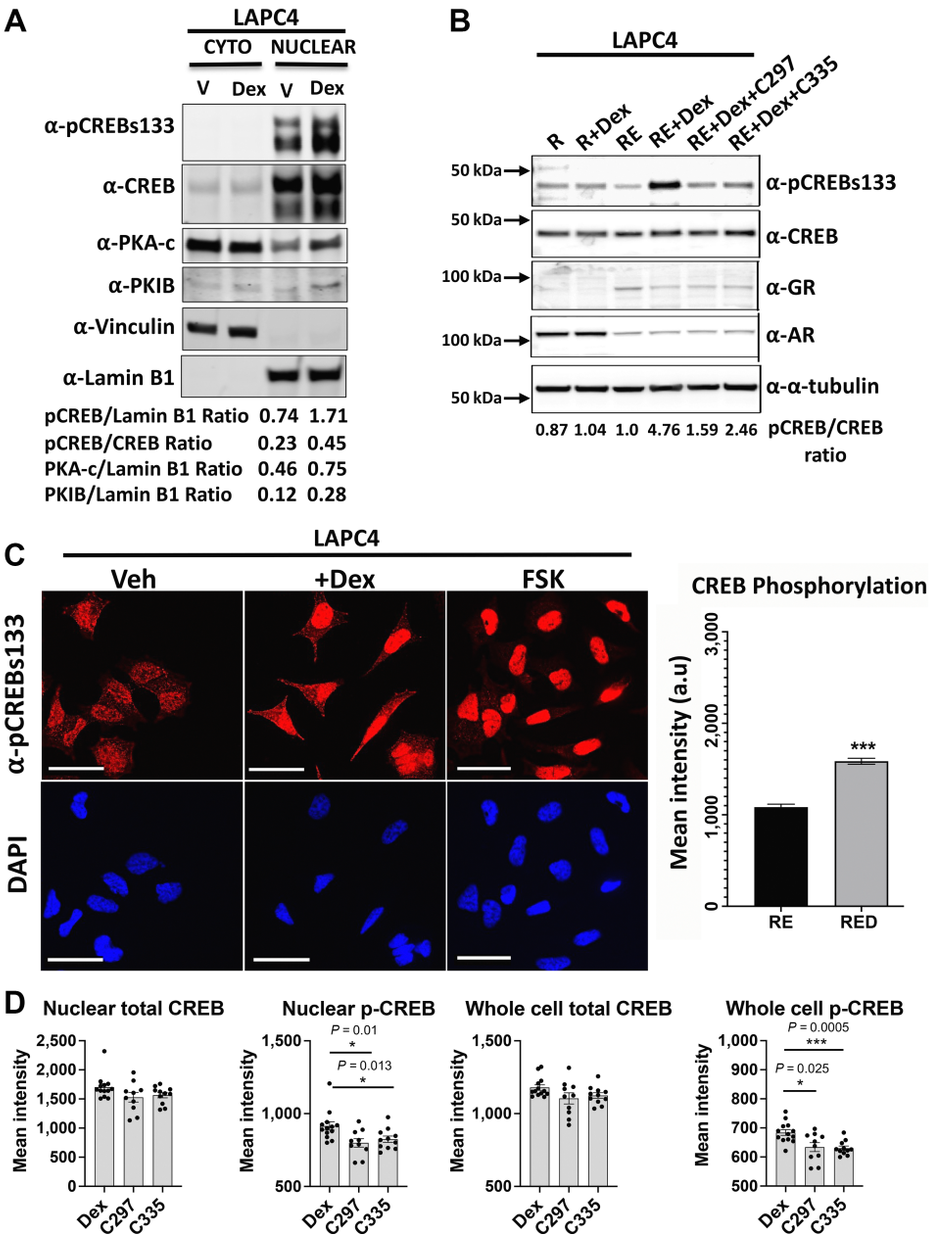

Figure 3.

A downstream cAMP-activated transcription factor, CREB, is phosphorylated at Ser133 following GR activation. **A,** Western blot of subcellular distribution of pCREBSer133, total CREB, PKA-c, and PKIB in LAPC4 cells cultured for 3 days in R1881 and enzalutamide (RE) media and then treated with Veh or Dex (8 hours). Densitometric analyses are listed below for each lane. **Figure 3A** is representative of three independent experiments. **B,** LAPC4 cells were cultured as above in RE media for 7 days, and then treated with either Veh, Dex, Dex+C297, Dex+C335 (8 hours) and a Western blot was performed. Densitometric analysis of phospho-CREB versus total CREB intensity is listed below each lane. The western blot shown is representative of three independent experiments. **C,** LAPC4 cells were cultured in RE media for 7 days, and then treated with either Veh or Dex (8 hours). Forskolin (FSK, 10 μmol/L) was used as a positive control for PKA-mediated CREB phosphorylation. Left, Cells were probed with α-pCREB-Ser133 antibody and stained with DAPI (600X magnification, scale bar = 25 μm). Right: Bar graph shows average CREB phosphorylation by mean immunofluorescent intensity per 8 to 13 FOVs; ***, $P < 0.001$ (Welch t test). **D,** Dot bar graphs (8–13 FOV per condition) show mean immunofluorescent intensity of whole cell or nuclear CREB and pCREB in LAPC4 cells.

co-treatment with dex + C297/C335 was followed by less pCREB compared with GR activation alone (**Fig. 3B**; Supplementary Fig. S4B), suggesting that GR activation is indeed upstream of CREBs133 phosphorylation.

We then used indirect immunofluorescent antibody staining to determine the effect of antagonizing GR activity with a SGRM on the subcellular localization of total and pCREB in both LAPC4 and CWR-22Rv1 cells. We found that in LAPC4 cells, GR antagonism resulted in decreased whole cell and nuclear CREB phosphorylation (**Fig. 3D**), whereas CWR-22Rv1 cells showed no significant difference in nuclear or whole cell CREB phosphorylation (Supplementary Fig. S4D). These results suggest that GR activation reliably increases total and nuclear CREB phosphorylation *in vitro* by western blot analysis. However, in CWR-22Rv1 cells, immunofluorescence pCREB microscopy may not be sensitive enough to detect SGRM antagonism of downstream CREB phosphorylation.

GR antagonism delays the development of enzalutamide resistance and inhibits PKIB expression in CRPC xenografts

We previously demonstrated that C297 and C335 inhibit GR-mediated proliferation of enzalutamide-treated prostate cancer cells but have not previously examined the effect of selective GR antagonism in the context of potent ARSi *in vivo* (6). Therefore, we examined whether the emergence of enzalutamide resistance in castration-resistant LAPC4 xenografts could be delayed by co-treatment with SGRMs C297 or C335 (**Fig. 4A**). We found that the addition of either SGRM C297 or C335 to enzalutamide treatment of CRPC significantly prolonged the time to tumor doubling of LAPC4 CRPC xenografts ($P < 0.0001$ for C335 and $P = 0.0032$ for C297). Next, we performed

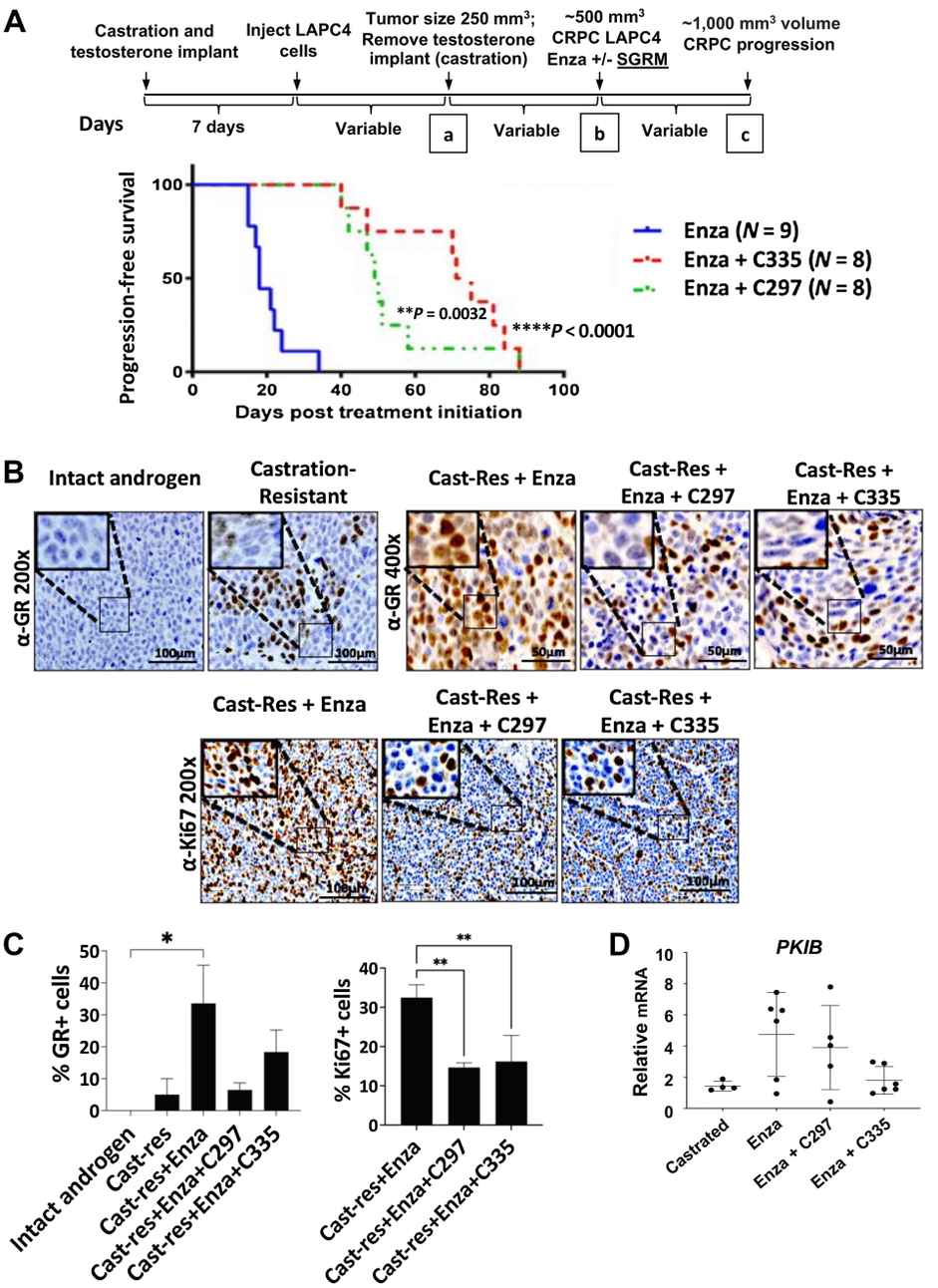

Figure 4.

Addition of SGRM to enzalutamide therapy delays tumor growth and inhibits *PKIB* expression in castration-resistant LAPC4 tumor xenografts. **A,** Schema of experiment shows that athymic nude mice underwent orchiectomy and immediate testosterone pellet implantation to allow initial LAPC4 xenograft growth. Following the establishment of primary LAPC4 xenograft tumors (in the presence of testosterone), removal of the testosterone pellet left castrate levels of androgen ("a"). Mice with resultant castration-resistant LAPC4 tumors (~500 mm^3) began treatment with ("b") enzalutamide (30 mg/kg chow), ± C297 (C297, 20 mg/kg/day), or C335 (C335, 20 mg/kg/day). Mice were sacrificed at tumor doubling (~1000 mm^3) which was considered CRPC progression ("c"). Below, Kaplan–Meier progression-free survival curves show time to CRPC doubling/progression. Log-rank *P* values are shown. **B,** LAPC4 representative anti-GR and anti-Ki67 immunohistochemistry with a magnified inset. **C,** Percentage of GR+ (left: *, $P < 0.05$; Welch *t* test) and Ki67+ cells (right: **, $P < 0.005$; Welch *t* test) shown for at least 3 tumors in each treatment group. **D,** Dot plot with mean and S.E.M of fold-change of *PKIB* mRNA measured by qRT-PCR from LAPC4 xenograft tumors normalized to reference gene (*ACTB*). $N = 7$–8 tumors per treatment.

GR immunohistochemistry on these xenografts, and samples were scored by a pathologist (RL) blinded to treatment conditions. As expected, treatment with enzalutamide following castration significantly increased tumor cell GR expression compared with tumors from non-castrated mice (34% vs. 0%; $P < 0.05$; **Fig. 4B** and **C**). Furthermore, enzalutamide co-treatment with C297 or C335 resulted in a significant decrease in Ki67+ cells compared with enzalutamide alone ($P = 0.0042$, 0.0065 respectively, **Fig. 4B** and **C**), consistent with the antiproliferative effects of GR antagonism in ARSi.

To determine *PKIB* expression levels in xenografted tumors from mice treated with enzalutamide alone versus enzalutamide with C297 or C335, *PKIB* mRNA was measured using q-RT-PCR. We found relatively increased steady-state *PKIB* transcript levels in tumors from castrated + enzalutamide-treated mice compared with castration alone as shown by the difference in mean expression (although not statistically significant due to small numbers of mice; **Fig. 4D**). Furthermore, co-treatment with enzalutamide and SGRM C335 or C297 resulted in a decrease in mean *PKIB* transcripts compared with enzalutamide alone. Taken together, these data suggest that GR-specific antagonism can inhibit cAMP/PKA-associated tumor gene expression and delay enzalutamide-resistant tumor progression *in vivo*.

cAMP signaling-associated gene expression is enriched in GR overexpressing metastatic patient CRPC samples

GR protein expression has been reported to be relatively upregulated in a subset of CRPC patient samples, although specific

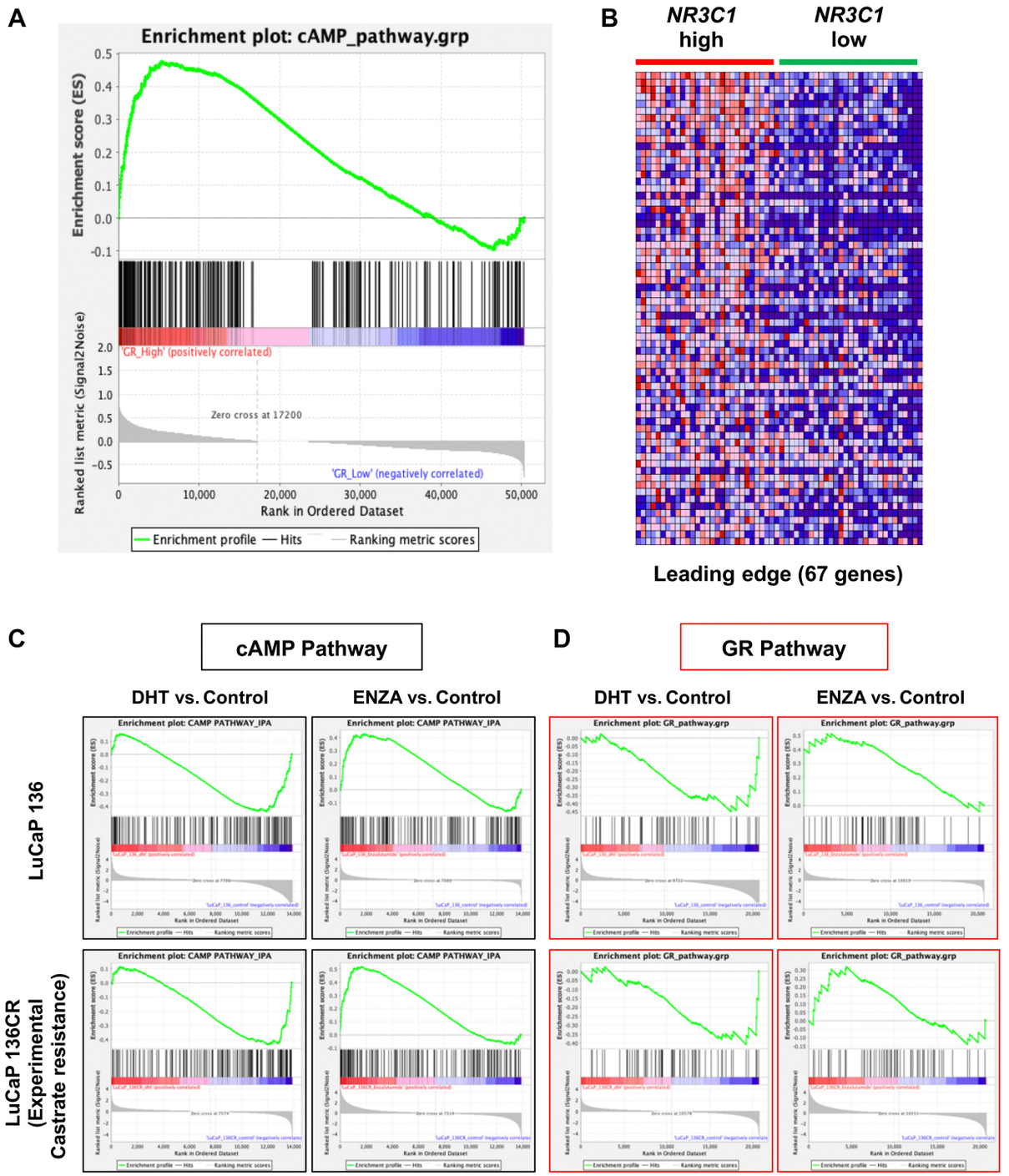

Figure 5.

mCRPC patient samples expressing high *NR3C1* (GR) mRNA transcripts show enrichment of cAMP signaling pathway gene expression. **A,** Enplot from GSEA for cAMP pathway genes using whole transcriptomic data from mCRPC patients ($n = 58$) expressing the highest and lowest levels of *NR3C1* (top and bottom quartiles; NES = 1.89; $P < 0.0001$). **B,** Heat map from GSEA analysis showing the 67 genes in the leading edge. The leading-edge subset can be interpreted as core gene expression that accounts for the gene set enrichment signal (http://www.gsea-msigdb.org/gsea/index.jsp). **C,** GSEA analyses for the cAMP pathway using transcriptomic data from LuCaP136 (top) or LuCaP136CR (experimental castration-resistant, bottom) PDX models exposed *in vivo* to either DHT (left) or enzalutamide (right) show decreased enrichment of the cAMP pathway with DHT (LuCaP136 NES = −1.039; $P < 0.001$; LuCaP136CR NES = −1.438; $P = 0.014$) and an increased enrichment following exposure to enzalutamide (LuCaP136 NES = 1.594; $P = 0.002$; LuCaP136CR NES = 1.441; $P = 0.008$). **D,** GSEA analyses for the GR pathway using transcriptomic data from LuCaP136 (top) or LuCaP136CR (experimental castration-resistant, bottom) PDX models exposed *in vivo* to DHT (left) or enzalutamide (right) show decreased enrichment of the GR pathway with DHT treatment (LuCaP136 NES = −1.099; $P = 0.32$; LuCaP136CR NES = −1.304; $P < 0.001$) and increased enrichment following exposure to enzalutamide (LuCaP136 NES = 1.378; $P = 0.07$; LuCaP136CR NES = 1.127; $P = 0.25$).

GR-mediated gene expression pathways have not been previously identified (29, 30). Given our evidence suggesting that cAMP/PKA signaling is a downstream pathway of GR signaling in AR-antagonized prostate cancer, we next investigated whether the cAMP signaling pathway is associated with high (versus low) GR expression in human mCRPC tumors. Using an updated RNA-seq dataset available on cBioPortal.org, GSEA revealed a significant enrichment of cAMP pathway genes was associated with higher *NR3C1* (*GR*) expression (**Fig. 5A** and **B**; Supplementary Fig. S5A; Supplementary Table S3). We also performed an analogous GSEA using gene expression data from PDX models of castration-sensitive (LuCaP 136) and CRPC (LuCaP 136CR) mice treated with either androgen (DHT) or enzalutamide (31). In these tumors, we found a significant enrichment of the cAMP signaling pathway with enzalutamide (ENZA) treatment but not with androgen (DHT) treatment (**Fig. 5C**). As expected, we also observed an enrichment in GSEA GR pathway gene expression in tumors resected following anti-AR enzalutamide treatment compared with tumors treated with androgen (DHT; **Fig. 5D**). Furthermore, GSEA analyses for cAMP or GR pathways with ENZA versus DHT (Supplementary Fig. S5B) also showed enrichment of cAMP and GR pathways with both castration-sensitive and castration-resistant PDX models. Taken together, these data are consistent with a model in which prostate cancer therapy with castration and AR antagonism results in GR activation and acquisition of a GR-specific transcriptome that includes the activation of cAMP/PKA signaling in human CRPC.

Discussion

The downstream oncogenic mechanisms that arise in prostate cancer following ARSi and subsequent GR activation that are acquired independently of AR-driven oncogenic pathways have not been well-delineated. This study suggests a novel role for this acquired GR activity in regulating downstream gene expression that can activate the cAMP/PKA signaling pathway. Analysis of the GR transcriptome following AR antagonism demonstrated that cAMP/PKA signaling is among the most significant and consistent GR-activated pathways. Furthermore, we found that GR activation increased the expression of PKIB, a PKA-interacting protein that promotes nuclear sequestration of PKA-c and phosphorylation of the known PKA substrate CREB. Furthermore, addition of SGRMs to enza in a CRPC model inhibited PKA activity *in vitro* and reduced tumor growth *in vivo*. Overall, these data support the conclusion that the acquisition of downstream cAMP/PKA signaling, a pathway known to be upregulated in CRPC (10, 32, 33), can be initiated by acquired GR transcriptional activity.

One of the interesting findings from our prostate cancer gene expression studies is that with both models, we found a subset of post-ARSi acquired GR-regulated genes that are shared with the AR transcriptome and another subset that is unique. We saw some overlap in these GR-unique versus AR-shared genes with the previous study of another prostate cancer cell line, LREX, described in Arora and colleagues (7). Specifically, we found a modest percentage (>25%) of LREX GR DEGs from this previous study in common with our study's GR-regulated genes from LAPC4 and 22RV1 cells (Supplementary Fig. S6A, left). A much smaller percentage (∼10%) of "selective" GR genes from Arora and colleagues overlapped with GR "unique" DEGs from this study (using the 1.6 fold cutoff of the Arora study, Supplementary Fig. S6B, left). Because the Arora and colleagues paper reported such a small number of GR DEGs (about 10% of our genes), the IPA gene expression pathways in Arora and colleagues were much less significant and could not be compared.

The predominant isoform of the cAMP-dependent PKI family of proteins, PKIA, inhibits PKA kinase activity by binding to its catalytic subunit (PKA-c). However, the beta isoform, PKIB, shares only 40% amino acid homology with PKIA and is markedly less potent in inhibiting PKA kinase activity (34). In fact, it has been shown that high expression of PKIB has a novel function, causing nuclear sequestration and increased activity of PKA-c, while knockdown of PKIB results in decreased nuclear PKA-c (27). In addition, overexpression of PKIB *in vitro* has been associated with increased proliferation and invasion of prostate cancer cells (27).

Our findings in CRPC models also expand our understanding of the crosstalk between GR signaling and cAMP/PKA activity (35–37). It has been shown in other cell lines that an increase in PKA activity can increase GR chromatin binding and transcriptional activity (38, 39). In light of our data revealing that GR can increase PKA activity in AR-antagonized prostate cancer, PKA activity may work together with activated GR in a feed-forward loop to promote CRPC progression.

In summary, these experiments reveal an ARSi context-dependent GR-specific regulation of cAMP/PKA/CREB activation suggesting that GR-induced PKA signaling may be an important mechanism underlying pCREB activation in CRPC. This discovery raises many additional questions regarding the crosstalk between GR and cAMP/PKA/pCREB. For instance, it is possible that additional non-genomic GR activities might also contribute to PKA activation through protein–protein interactions, as occurs with non-genomic GR activation of MAPK signaling (40). It is still unclear how AR blockade alters GR chromatin association and transcriptomic activity in CRPC, although one possibility is through conformational changes in the ratios of AR and GR shared transcription factor complex proteins and pioneer factors (e.g., FOXA1) that could alter GR chromatin accessibility following AR antagonism (41). Alternatively, therapeutic AR antagonism could act as a prostate cancer cell stressor, leading to kinase activation (31) and alternative GR posttranslational modification and transcriptomic output. Ongoing studies will further define the relationship between AR antagonism and subsequent activation of GR and cAMP/PKA/CREB signaling, thereby providing mechanistic insight into pathways that require GR activity and refine the potential of GR antagonism in CRPC.

Authors' Disclosures

R.Z. Szmulewitz reports coinventor with S.D. Conzen of a patent issued to The University of Chicago for methods and compositions related to GR antagonists and prostate cancer. S.D. Conzen reports coinventor with R.Z. Szmulewitz of a patent issued to The University of Chicago for methods and compositions related to GR antagonists and prostate cancer. No disclosures were reported by the other authors.

Authors' Contributions

L. Bennett: Conceptualization, data curation, formal analysis, supervision, validation, visualization, methodology, writing–original draft, project administration, writing–review and editing. **P.K. Jaiswal:** Formal analysis, investigation. **R.V. Harkless:** Data curation, formal analysis, validation, investigation, project administration. **T.M. Long:** Formal analysis, investigation, methodology, project administration. **N. Gao:** Data curation, formal analysis, investigation, visualization. **B. Vandenburg:** Conceptualization, data curation, formal analysis, investigation, visualization. **P. Selman:** Data curation, formal analysis, investigation. **I. Durdana:** Formal analysis, validation. **R.R. Lastra:** Formal analysis, validation, investigation. **D. Vander Griend:** Conceptualization, formal analysis, supervision, writing–review and editing. **R. Adelaiye-Ogala:** Formal analysis, funding acquisition, validation, investigation, methodology, writing–original draft, writing–review and editing. **R.Z. Szmulewitz:** Conceptualization, resources, data curation, formal analysis, supervision, funding acquisition, validation, visualization, methodology, writing–

original draft, project administration, writing–review and editing. **S.D. Conzen:** Conceptualization, data curation, formal analysis, supervision, funding acquisition, validation, investigation, visualization, methodology, writing–original draft, project administration, writing–review and editing.

Acknowledgments

This study was supported by the Northwestern-University of Chicago Prostate SPORE 1P50CA180995 (to S.D. Conzen and R.Z. Szmulewitz), Stewart J. Rahr Foundation - Prostate Cancer Foundation (PCF) Challenge Award (to S.D. Conzen and R.Z. Szmulewitz). S.D. Conzen is also supported by Cancer Prevention and Research Institute of Texas Established Scholar award #RR190037. R. Adelaiye-Ogala is supported by a Department of Defense, CDMRP-PCRP Early Investigator (W81XWH-19–1-0715) and the Prostate Cancer Foundation.

We thank Drs. Hazel Hunt, Andy Greenstein, Robert Roe, and Stacie Shepherd for sharing their expertise with GR modulators and Astellas Pharma Global Development, Inc/Pfizer for enzalutamide drug support. We thank Dr. Nic Dulin of The University of Chicago for early helpful discussions on PKA regulation. We also thank Cydney Sutherland for excellent assistance in the preparation of the manuscript.

Note

Supplementary data for this article are available at Molecular Cancer Therapeutics Online (http://mct.aacrjournals.org/).

Received April 12, 2023; revised September 4, 2023; accepted November 27, 2023; published first November 29, 2023.

References

1. Siegel RL, Miller KD, Wagle NS, Jemal A. Cancer statistics, 2023. CA Cancer J Clin 2023;73:17–48.
2. Huggins C, Stevens RJ, Hodges C. Studies on prostatic cancer. II. The effects of castration on advanced carcinoma of the prostate gland. Arch Surg 1941;43: 209–23.
3. Scardino PT, Linehan WM, Zelefsky MJ, Vogelzang NJ, Rini BI, Bochner BH, Sheinfeld J, editors. Comprehensive textbook of genitourinary oncology. Philadelphia: Lippincott Williams & Wilkins; 2006. xxix, 907 p. 8.
4. Scher HI, Fizazi K, Saad F, Taplin M-E, Sternberg CN, Miller K, et al. Effect of MDV3100, an androgen receptor signaling inhibitor (ARSI), on overall survival in patients with prostate cancer postdocetaxel: results from the phase III AFFIRM study. J Clin Oncol 2012;30:LBA1.
5. Kregel S, Chen JL, Tom W, Krishnan V, Kach J, Brechka H, et al. Acquired resistance to the second-generation androgen receptor antagonist enzalutamide in castration-resistant prostate cancer. Oncotarget 2016;7:26259–74.
6. Isikbay M, Otto K, Kregel S, Kach J, Cai Y, Vander Griend DJ, et al. Glucocorticoid receptor activity contributes to resistance to androgen-targeted therapy in prostate cancer. Horm Cancer 2014;5:72–89.
7. Arora VK, Schenkein E, Murali R, Subudhi SK, Wongvipat J, Balbas MD, et al. Glucocorticoid receptor confers resistance to antiandrogens by bypassing androgen receptor blockade. Cell 2013;155:1309–22.
8. Wu W, Chaudhuri S, Brickley DR, Pang D, Karrison T, Conzen SD. Microarray analysis reveals glucocorticoid-regulated survival genes that are associated with inhibition of apoptosis in breast epithelial cells. Cancer Res 2004;64:1757–64.
9. Kach J, Long TM, Selman P, Tonsing-Carter EY, Bacalao MA, Lastra RR, et al. Selective glucocorticoid receptor modulators (SGRMs) delay castrate-resistant prostate cancer growth. Mol Cancer Ther 2017;16:1680–92.
10. Pollack A, Bae K, Khor LY, Al-Saleem T, Hammond ME, Venkatesan V, et al. The importance of protein kinase A in prostate cancer: relationship to patient outcome in radiation therapy oncology group trial 92–02. Clin Cancer Res 2009;15:5478–84.
11. Li J, Alyamani M, Zhang A, Chang KH, Berk M, Li Z, et al. Aberrant corticosteroid metabolism in tumor cells enables GR takeover in enzalutamide resistant prostate cancer. eLife 2017;6:e20183.
12. Dobin A, Davis CA, Schlesinger F, Drenkow J, Zaleski C, Jha S, et al. STAR: ultrafast universal RNA-seq aligner. Bioinformatics 2013;29:15–21.
13. Wang L, Wang S, Li W. RSeQC: quality control of RNA-seq experiments. Bioinformatics 2012;28:2184–5.
14. Trapnell C, Williams BA, Pertea G, Mortazavi A, Kwan G, van Baren MJ, et al. Transcript assembly and quantification by RNA-Seq reveals unannotated transcripts and isoform switching during cell differentiation. Nat Biotechnol 2010;28: 511–5.
15. Liao Y, Smyth GK, Shi W. featureCounts: an efficient general purpose program for assigning sequence reads to genomic features. Bioinformatics 2014;30: 923–30.
16. Love MI, Huber W, Anders S. Moderated estimation of fold change and dispersion for RNA-seq data with DESeq2. Genome Biol 2014;15:550.
17. Robinson MD, McCarthy DJ, Smyth GK. edgeR: a bioconductor package for differential expression analysis of digital gene expression data. Bioinformatics 2010;26:139–40.
18. Pflueger D, Terry S, Sboner A, Habegger L, Esgueva R, Lin PC, et al. Discovery of non-ETS gene fusions in human prostate cancer using next-generation RNA sequencing. Genome Res 2011;21:56–67.
19. Robinson D, Van Allen EM, Wu YM, Schultz N, Lonigro RJ, Mosquera JM, et al. Integrative clinical genomics of advanced prostate cancer. Cell 2015;161: 1215–28.
20. Subramanian A, Tamayo P, Mootha VK, Mukherjee S, Ebert BL, Gillette MA, et al. Gene set enrichment analysis: a knowledge-based approach for interpreting genome-wide expression profiles. Proc Natl Acad Sci USA 2005;102: 15545–50.
21. Michiel Sedelaar JP, Dalrymple SS, Isaacs JT. Of mice and men–warning: intact versus castrated adult male mice as xenograft hosts are equivalent to hypogonadal versus abiraterone treated aging human males, respectively. Prostate 2013; 73:1316–25.
22. Bankhead P, Loughrey MB, Fernández JA, Dombrowski Y, McArt DG, Dunne PD, et al. QuPath: open source software for digital pathology image analysis. Sci Rep 2017;7:16878.
23. Hunt HJ, Belanoff JK, Golding E, Gourdet B, Phillips T, Swift D, et al. 1H-Pyrazolo[3,4-g]hexahydro-isoquinolines as potent GR antagonists with reduced hERG inhibition and an improved pharmacokinetic profile. Bioorg Med Chem Lett 2015;25:5720–5.
24. Hunt HJ, Ray NC, Hynd G, Sutton J, Sajad M, O'Connor E, et al. Discovery of a novel non-steroidal GR antagonist with *in vivo* efficacy in the olanzapine-induced weight gain model in the rat. Bioorg Med Chem Lett 2012;22:7376–80.
25. Kramer A, Green J, Pollard J Jr., Tugendreich S. Causal analysis approaches in ingenuity pathway analysis. Bioinformatics 2014;30:523–30.
26. Hassan S, Pullikuth A, Nelson KC, Flores A, Karpova Y, Baiz D, et al. β2-adrenoreceptor signaling increases therapy resistance in prostate cancer by upregulating MCL1. Mol Cancer Res 2020;18:1839–48.
27. Chung S, Furihata M, Tamura K, Uemura M, Daigo Y, Nasu Y, et al. Overexpressing PKIB in prostate cancer promotes its aggressiveness by linking between PKA and Akt pathways. Oncogene 2009;28:2849–59.
28. Pan W, Zhang Z, Kimball H, Qu F, Berlind K, Stopsack KH, et al. Abiraterone acetate induces CREB1 phosphorylation and enhances the function of the CBP-p300 complex, leading to resistance in prostate cancer cells. Clin Cancer Res 2021;27:2087–99.
29. Szmulewitz RZ, Chung E, Al-Ahmadie H, Daniel S, Kocherginsky M, Razmaria A, et al. Serum/glucocorticoid-regulated kinase 1 expression in primary human prostate cancers. Prostate 2012;72:157–64.
30. Yemelyanov A, Bhalla P, Yang X, Ugolkov A, Iwadate K, Karseladze A, et al. Differential targeting of androgen and glucocorticoid receptors induces ER stress and apoptosis in prostate cancer cells: a novel therapeutic modality. Cell Cycle 2012;11:395–406.
31. Adelaiye-Ogala R, Gryder BE, Nguyen YTM, Alilin AN, Grayson AR, Bajwa W, et al. Targeting the PI3K/AKT pathway overcomes enzalutamide resistance by inhibiting induction of the glucocorticoid receptor. Mol Cancer Ther 2020;19: 1436–47.
32. Moen LV, Ramberg H, Zhao S, Grytli HH, Sveen A, Berge V, et al. Observed correlation between the expression levels of catalytic subunit, Cbeta2, of cyclic adenosine monophosphate—dependent protein kinase and prostate cancer aggressiveness. Urol Oncol 2017;35:111.e1–8.

33. Khor LY, Bae K, Al-Saleem T, Hammond EH, Grignon DJ, Sause WT, et al. Protein kinase A RI-alpha predicts for prostate cancer outcome: analysis of radiation therapy oncology group trial 86–10. Int J Radiat Oncol Biol Phys 2008; 71:1309–15.
34. Dalton GD, Dewey WL. Protein kinase inhibitor peptide (PKI): a family of endogenous neuropeptides that modulate neuronal cAMP-dependent protein kinase function. Neuropeptides 2006;40:23–34.
35. Kvissel AK, Ramberg H, Eide T, Svindland A, Skålhegg BS, Taskén KA. Androgen dependent regulation of protein kinase A subunits in prostate cancer cells. Cell Signal 2007;19:401–9.
36. Cox ME, Deeble PD, Lakhani S, Parsons SJ. Acquisition of neuroendocrine characteristics by prostate tumor cells is reversible: implications for prostate cancer progression. Cancer Res 1999;59:3821–30.
37. Bang YJ, Pirnia F, Fang WG, Kang WK, Sartor O, Whitesell L, et al. Terminal neuroendocrine differentiation of human prostate carcinoma cells in response to increased intracellular cyclic AMP. Proc Natl Acad Sci USA 1994;91:5330–4.
38. Rangarajan PN, Umesono K, Evans RM. Modulation of glucocorticoid receptor function by protein kinase A. Mol Endocrinol 1992;6:1451–7.
39. Eickelberg O, Roth M, Lorx R, Bruce V, Rudiger J, Johnson M., et al. Ligand-independent activation of the glucocorticoid receptor by beta2-adrenergic receptor agonists in primary human lung fibroblasts and vascular smooth muscle cells. J Biol Chem 1999;274:1005–10.
40. Kadmiel M, Cidlowski JA. Glucocorticoid receptor signaling in health and disease. Trends Pharmacol Sci 2013;34:518–30.
41. Pihlajamaa P, Sahu B, Jänne OA. Determinants of receptor- and tissue-specific actions in androgen signaling. Endocr Rev 2015;36:357–84.